Image Cover Sheet

CLASSIFICATION	SYSTEM NUMBER
UNCLASSIFIED	517054

TITLE

Lidar monitoring of clouds

System Number:

Patron Number:

Requester:

Notes:

DSIS Use only:

Deliver to: CL

This page is left blank

This page is left blank

PROCEEDINGS OF SPIE REPRINT

SPIE—The International Society for Optical Engineering

Reprinted from

Remote Sensing of Clouds and the Atmosphere VI

17–20 September 2001
Toulouse, France

SPIE P PROCEEDINGS SERIES

Volume 4539

Lidar Monitoring of Clouds

Luc R. Bissonnette* and Gilles Roy†
Defence Research Establishment Valcartier (DREV)
2459 Pie-XI Blvd. North, Val-Bélair, QC G3J 1X5, Canada
and
Stewart G. Cober‡ and George A. Isaac§
Meteorological Service of Canada
4905 Dufferin Street, Toronto, ON M3H 5T4, Canada

ABSTRACT

The lidar has long been proposed as a potential remote sensor of cloud microphysical and optical parameters. The conventional lidar has had only mixed success because retrieval in a medium of such density requires an independently measured boundary value deep in the cloud and a relation between basckscatter and extinction The solution we propose is to make detection at multiple fields of view (MFOV) and exploit the additional information provided by multiple scattering. In this paper, we compare MFOV-based lidar retrievals with *in situ* measurements of the liquid water content and droplet diameters in liquid-phase stratus clouds. The results show good correlation between the lidar solutions and the *in situ* data, but a constant bias of 20-30% depending on the parameter. The bias is reduced to 10% if comparisons are restricted to the cloud base region accessible to the lidar. Another significant conclusion is that the lidar solutions are, within 20-30%, statistically representative of the complete layer in spite of the limited penetration range.
Keywords: lidar, multiple scattering, clouds

1. INTRODUCTION

There is a growing need for the development of reliable and practical means of measuring cloud parameters remotely. Remote sensors allow long-term monitoring at low cost and often with high spatial and temporal resolution. This is important to support the development of cloud models and to understand their role on the earth radiation budget and global climate.

The lidar is an effective cloud sensor. Its short wavelength makes it particularly sensitive to the small fog and cloud droplets. For comparison, mm-wave radar reflectivity is proportional to the sixth order moment of the droplet size distribution[1] whereas lidar backscatter scales as the second order moment. However, conventional lidar retrieval techniques have had mixed success in dense media such as fog and clouds. One reason is that the backscatter and extinction coefficients have comparable effects on the measured signal which makes it necessary to make additional measurements or to assume a relation between backscatter and extinction. The second reason has to do with the nonlinearity of the governing equation which, for the stability of the solution, requires a boundary value at the far end of the lidar range where it is least likely to be known with accuracy. Over the past years, our group has been working on a multiple-field-of-view (MFOV) lidar method[2,3] designed to make use of the additional information contained in the multiple scattering contributions.[4] The primary solution products are the range-resolved extinction coefficient and the effective droplet diameter from which properties such as the cloud liquid water content can de derived. More details and preliminary solution results are given in Bissonnette *et al.*.[5]

Recently, we operated our MFOV lidar at a site that was vertically and horizontally probed for periods of 2-3 hours at a time by an aircraft instrumented with a multitude of sensors to measure droplet size spectra and liquid water content. The data collected during those experiments constitute the best validation test for our

*luc bissonnette@drev dnd.ca; phone 418-844-4000 x4437; fax 418-844-4511
†gilles roy@drev.dnd ca, phone 418-844-4000 x4335, fax 418-844-4511
‡stewart cober@ec gc.ca
§george isaac@ec gc.ca

Remote Sensing of Clouds and the Atmosphere VI, Klaus Schafer, Olga Lado-Bordowsky, Adolfo Comeron, Michel R. Carleer, Janet S. Fender, Editors, Proceedings of SPIE Vol. 4539 (2002) © 2002 SPIE · 0277-786X/02/$15 00

lidar method. They were collected as close as possible to the lidar site with excellent resolution of the cloud vertical structure. Horizontally, the area covered remained representative of what the lidar was sampling during the one-hour-plus periods of simultaneous lidar-aircraft measurements.

The comparisons of this paper are between *in situ* aircraft measurements and lidar retrievals of cloud microphysical properties for simultaneous measurement periods in liquid-phase clouds. Our purpose is to test the MFOV lidar retrieval method, and to determine how representative of the complete cloud layer are the lidar solutions limited to the bottom region of the cloud because of signal fading. We are not concerned here with cloud physics issues. Our main preoccupation is the precision with which cloud physical and optical properties can be remotely determined with an MFOV lidar.

2. INVERSION METHOD

In dense particulate media, lidar measurements at wavelengths smaller than the effective particle size are significantly affected by multiple scattering. We have developed at DREV a lidar receiver that measures and angularly resolves these multiple-scattering contributions. Two different implementations of our MFOV receiver have been described in a number of publications (Refs. 2-8).

The direct problem of predicting multiply scattered lidar returns given the medium properties is now well understood and accurately solved, particularly by numerical Monte Carlo simulations.[9] However, the inverse problem of retrieving the medium properties from lidar measurements still constitutes a challenging task. The multiple-scattering contributions are the result of repeated integrated interactions over the complete lidar path as clearly illustrated by the model of Eloranta.[10] Inverting these integrals for determining local parameters through rigorous analytical techniques is clearly daunting. In addition to the mathematical complexity of inverting such expressions, one has to deal with the difficult problems of uniqueness and stability of the solutions because of the intrinsic nonlinearity. We use here a less rigorous and necessarily less precise solution method, but one that circumvents these difficulties with a good degree of robustness. The method is described at length in Bissonnette *al.*[11]: we give here only a brief outline.

The solution technique has three main features: a droplet size algorithm, an initialization procedure for the extinction coefficient, and the extinction solution.

The retrieval of droplet size is based on the field-of-view (FOV) dependence of the measured MFOV returns $P(z,\theta)$, where z is the range and θ is the FOV We have developed a simple model of the θ-dependence of $P(z,\theta)$ for the purpose of solving for the droplet diameter. According to this model, the FOV scale θ_m is determined at each range z by fitting the measured $P(z,\theta)$ to the function

$$P(z,\theta) \;=\; A \;+\; B\,\Phi(\theta/\theta_m)\,, \tag{1}$$

where Φ is the error function, and A, B and θ_m are the free parameters determined by the least squares fit. The function Φ was chosen because it is simple and was found to represent well the θ-dependence of $P(z,\theta)$. The droplet size information is contained in the field-of-view scale θ_m. However, the value of θ_m results from forward diffraction scatterings that are droplet size dependent, and refraction/reflection scatterings that are independent of droplet size. It is therefore necessary to extract the diffraction part θ_{md} from θ_m. We do this by successively fitting Eq. 1 to the measured $P(z,\theta)$, the calculated diffraction-alone $P(z,\theta)$ and the calculated total $P(z,\theta)$, and substituting the results in the simple expression

$$\theta_{md} \;=\; \frac{\theta_{cd}}{\theta_{ct}}\,\theta_m\,, \tag{2}$$

where θ_{cd}, θ_{ct} and θ_m are the scales derived from the fits to the calculated diffraction-alone, calculated total and measured $P(z,\theta)$, respectively. The calculations are carried out with the model of Ref. 2 using the solutions obtained at all ranges preceding the current range z. Finally, the effective droplet diameter d_e is obtained from the expression

$$d_e(z) \;\simeq\; 0.585\lambda\sqrt{\frac{2n(\tau)\,(z-z^-)}{(z+z^-)\,[\theta_{md}^2(z)+\theta_{md}^2(z^-)]}}\,, \tag{3}$$

where λ is the lidar wavelength, z is the current range, z^- is the range one optical depth ahead of z, $n(\tau) = 1$ or τ depending on whether τ is smaller or greater than unity, and τ is the optical depth at z.

The droplet size retrieval algorithm defined by Eqs. 1–3 is mostly empirical. A formal theoretical basis and improvements are still being investigated.

The extinction solution is initialized in the range interval that satisfies the relation

$$1.3 \leq \frac{P(z,\theta_{max})}{P(z,\theta_{min})} \leq 1.5, \tag{4}$$

where θ_{max} and θ_{min} are the system maximum and minimum FOVs, respectively. The minimum FOV is chosen just slightly greater than the beam divergence. For cloud studies at a range of 100 m to 2000-3000 m, θ_{max} should be of the order of 10-12 mrad, full angle. In the interval defined by Eq. 4, we have from a second order scattering estimate and Monte Carlo calculations that the optical depth is well approximated by

$$\tau(z) \simeq \frac{1}{\delta}\left\{\frac{P(z,\theta_{max}) - P(z,\theta_{min})}{P(z,\theta_{min})}\right\}, \tag{5}$$

where δ is the relative backscatter coefficient for angles close to 180°, it is measured relative to the value at exactly 180°. Typically $\delta \simeq 0.7$. Equation 5 allows for the estimation of the optical depth in the interval defined by Eq. 4 from the measured relative strength of the multiple scattering contributions. For Eq. 5 to be applicable, (z,θ_{max}) must be such that $P(z,\theta_{max})$ is nearing the asymptotic value of $P(z,\theta)$ for large θ. Next, we use the $\tau(z)$ derived from Eq. 5 and the effective diameter calculated from Eq. 3 to calibrate the lidar signals. Then, we choose inside the interval of Eq. 4 the range z_{ini} that is closest to the signal maximum and we solve for the extinction coefficient α at all ranges $z < z_{ini}$, where multiple scattering is small to negligible, using the backward-integration Klett method[12] with $\tau(z_{ini})$ obtained from Eq. 5 as the boundary value. The calculation of the calibration constant and of the solution $\alpha(z \leq z_{ini})$ completes the initialization.

To proceed with the extinction solutions at ranges $z > z_{ini}$, we need the multiple scattering lidar equation which we write as follows

$$P(z,\theta) = K\frac{k(z)}{z^2}\alpha(z)\,M(z,\tau,\theta)\,\exp[-2\tau(z)], \tag{6}$$

where K is the calibration constant obtained at initialization, $k(z)$ is the backscatter-to-extinction ratio estimated from the size solution, $\alpha(z)$ is the extinction coefficient we want to solve for, and $M(z,\tau,\theta)$ is the lidar multiple-to-single scattering ratio. Upon incrementing z, the values of $\alpha(z)$ and $\tau(z)$ are extrapolated from the solutions at the preceding step. Then, we sequentially calculate the droplet size $d_e(z)$, the backscatter-to-extinction ratio $k(z)$ and the multiple scattering functions $M(z,\tau,\theta)$ using the last updated $d_e(z)$ and $\alpha(z)$ and the solutions already derived for all ranges less than z. These calculations are performed using the size retrieval algorithm of Eq. 3, a Mie code and the multiple scattering model of Ref. 2. Finally, the extinction coefficient is updated by substituting all these quantities in the multiple scattering lidar equation, or more precisely, in the expression

$$\alpha(z) = \frac{1}{K}\frac{z^2}{k(z)}e^{2\tau(z)}\frac{M(z,\tau,\theta_{min})}{M^2(z,\tau,\theta_{max})}\frac{P^2(z,\theta_{max})}{P(z,\theta_{min})}. \tag{7}$$

Equation 7 is actually the solution for the backscattering coefficient transformed into the extinction coefficient $\alpha(z)$ by the Mie calculated ratio $k(z)$. This is done because it is through the backscattering coefficient that the lidar returns depend most on local cloud properties. The solution is written in terms of the ratio $P^2(z,\theta_{max})/P(z,\theta_{min})$ instead of $P(z,\theta)$ because, formulated in this fashion, the multiple scattering terms counterbalance more effectively the amplifying exponential term $\exp(2\tau)$ that would otherwise cause fatal instabilities. Once $\alpha(z)$ is calculated, we go back to the solution of $d_e(z)$ and repeat all calculations until the new $d_e(z)$ and $\alpha(z)$ differ from the preceding ones by less than preset margins.

After convergence is attained, we proceed forward to the next range bin and restart the iterations. We terminate the solutions where $P(z,\theta_{min})$ reaches the instrument noise level. We thus obtain range-resolved solutions for the effective droplet diameter and the extinction coefficient over the complete lidar range defined by a valid signal in the smallest field of view.

From the definition of the extinction coefficient

$$\alpha = \frac{\pi}{4} \int_0^\infty \frac{\mathrm{d}N}{\mathrm{d}d} Q_e(d,\lambda)\, d^2\, \mathrm{d}d, \tag{8}$$

where $\mathrm{d}N/\mathrm{d}d$ is the droplet diameter probability density function and $Q_e(d,\lambda)$ is the Mie extinction efficiency factor: plus the definition of the liquid water content(LWC)

$$\mathrm{LWC} = \frac{4\pi}{24} \rho \int_0^\infty \frac{\mathrm{d}N}{\mathrm{d}d} d^3\, \mathrm{d}d, \tag{9}$$

where ρ is the density of liquid water; and the model $Q_e(d,\lambda) \simeq 2$ valid for cloud droplets at our lidar wavelength of 1.06 μm, we obtain

$$\mathrm{LWC}(z) = \frac{1}{3} \rho\, \alpha(z)\, d_e(z), \tag{10}$$

where the effective diameter d_e is the ratio of the third- to the second-order moments of $\mathrm{d}N/\mathrm{d}d$. Hence, the LWC is to a good approximation proportional to the product of the two primary solutions of our MFOV lidar retrieval method.

3. EXPERIMENT

The experiment, designated as the Alliance Icing Research Study (AIRS), took place at Mirabel, Québec in the winter of 1999-2000. The main objectives were the characterization of cloud and precipitation conditions leading to in-flight icing of aircraft, and the testing of potential remote sensors of icing hazard. The program brought together various groups to perform coordinated remote and *in situ* measurements of clouds and precipitation over extended periods of time and under conditions propitious to icing. An overview of the complete program was presented elsewhere.[13]

A primary objective of the lidar participation in AIRS was the validation of the MFOV retrieval method. The AIRS experiment was particularly well suited for this task. The lidar and the other remote sensing equipments were located at Mirabel airport within a few hundred meters from the main runway. The instrumented aircraft participating in the experiment flew various flight patterns consisting of horizontal level passes at different altitudes above the runways, spirals centered on the remote sensors, and missed approaches. In other words, the cloud layer at the site was thoroughly probed vertically and horizontally for periods of 1-3 hours at a time. We compare in this paper our lidar retrieval solutions with the aircraft *in situ* measurements.

Our MFOV lidar is an Nd:YAG system with the following specifications: 1.06-μm wavelength, 70-mJ pulse energy, 12-ns pulse duration, 25-mm beam diameter at the transceiver, 0.5-mrad beam divergence, selectable pulse repetition frequency up to 100 Hz, 200-mm diameter telescope receiver co-linear with the laser axis, and variable fields of view (FOV). The FOVs are changed at the chosen laser repetition frequency of 100 Hz by rotating a 125-mm diameter aluminized glass disk with apertures of different sizes etched on a peripheral circle at equidistant angular intervals. The disk is positioned in the image plane of the main telescope mirror. The laser Q-switch is slaved to the disk rotation velocity to insure that the FOV apertures are in position on the lidar axis in synchronization with the laser pulses. The disk has 32 apertures defining 32 FOVs between 0.1 and 12 mrad, full angle. A complete FOV scan takes 32/100 s during which time it is assumed that the cloud remains unchanged.

The lidar was operated in a vertical stare mode. Bursts of 1000 pulses were fired, at the laser repetition rate of 100 Hz, every minute for periods of 1-3 hours. For each burst, we therefore have $1000 \div 32 = 31$ complete sets of MFOV returns spanning a time interval of 10 s The MFOV retrieval method requires only one of those sets which corresponds to a 1/3-s snapshot of the cloud. To minimize fluctuation errors, we generally average over 6 s or 18 consecutive MFOV sets. We decided on 6 s because we drop the first 3 s of the bursts to allow good thermalization of the laser Halving the averaging time produced very little difference in the retrieved values; in other words the 6-s averaging time is not a critical parameter.

The primary solution results for each burst are the profiles of the extinction coefficient $\alpha(z)$ and the effective droplet size $d_e(z)$, where z is height above ground. The relevant cloud microphysical parameters measured by the aircraft that we can compare with lidar retrievals are the liquid water content (LWC) and the droplet diameter. We therefore use Eq. 10 to derive LWC from $\alpha(z)$ and $d_e(z)$.

4. COMPARISON RESULTS

It is obvious that the comparisons between the aircraft and the lidar data cannot be done on a point-by-point basis. The lidar spatial resolution is a cube of typically 2 m on the sides whereas each aircraft sensor sweeps a sampling volume of the order of a few cm wide by $\sim$ 100 m long for the highest temporal resolution of 1 s. In addition, the aircraft flies in the general airport area covering tens of km while the lidar probes the cloud in a fixed vertical column. However, averages are comparable if the cloud is relatively steady and homogeneous.

Cloud profiles are of special interest. Because the aircraft has no instantaneous cloud base reference, profile comparisons are possible only if the cloud base is uniform and stable. One aircraft parameter suitable for profile comparison is the LWC measured at intervals of 1 s by the King and Nevzorov hotwire sensors Figure 1 is a plot of the LWC profiles measured by the aircraft King probe and the lidar for the period of 20h50-21h50 on 3 December 1999 during which the cloud base height varied by less than 100 m. The aircraft altitude data is referenced to the average cloud base height for the period, i.e. 1060 m, whereas the lidar data is with respect to the base value determined for each lidar burst. Figure 1 shows the one-hour averaged profiles and the instantaneous data, actually only a sample of the complete set to avoid overcrowding an already busy graph. The average curves fall almost exactly on top of one another indicating good statistical agreement. The instantaneous data points, however, are very much scattered illustrating the impracticability of doing point-by-point comparisons. The aircraft data scatter is less below 200 m and more tightly distributed about the average curve. The explanation is that the aircraft sampling is limited in that region to only two short passes through the cloud base. For longer dwell times, such as at 250 m, 480 m and 670 m, the scatter of the aircraft data is of the same order as that of the lidar solutions. In summary, Fig. 1 shows good agreement for the mean profiles and the amount of statistical fluctuations.

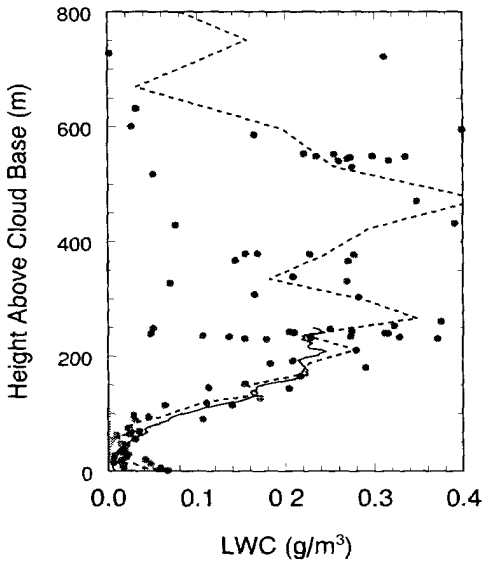

FIGURE 1 –Average and instantaneous LWC profiles for the period 20h50-21h50 UTC on 3 December 1999. The continuous line that ends at 250 m is the average lidar profile; the broken line that extends up to 800 m is the average King probe profile: the pluses are the instantaneous lidar solutions; and the solid disks are the King probe instantaneous measurements.

Overall, the profile comparisons show good general agreement. The fit is not everywhere as good as in Fig. 1 and there are local differences that can reach 100%. However, this is not unreasonable considering that the cloud base at the vertical of the aircraft measurements is only estimated and that the King probe averages in the cloud base region are the results of only brief periods when the aircraft flew in and out of the clouds.

Profile comparisons such as illustrated in Fig 1 are always open to interpretation because of the unavoidable temporal and spatial separations between the data sets. However, for the stratus clouds studied in this report, it is reasonable to assume statistical horizontal homogeneity over scales of a few tens of km and statistical stationarity over periods of 1-2 hours. Under such conditions, it is justifiable to compare the statistics of parameters measured at different positions and times within the acceptable homogeneous and stationary domain. In these comparisons, we use the 30-s averages of the King and Nevzorov LWC measurements because they are better quality controlled than the 1-s data. For droplet size, we use the 30-s full droplet diameter spectra derived

from the aircraft-mounted Particle Measuring Systems (PMS) forward scattering spectrometers FSSP 096 (3–45 μm) and FSSP 124 (5–95 μm), and particle imaging probe 2DC (25–800 μm) or 2DG (25–1600 μm). We calculate the effective droplet diameter and LWC directly from the spectra. To make sure that we retain only in-cloud data for our comparisons, we disregard all measurements with LWC < 0.02 g/m^3. In the case of the lidar, since we have for each measurement the height of the cloud base, we additionally remove the points that are less than 20 m from cloud base. We further degrade the height resolution of the remaining solution points to 20 m to insure statistical decorrelation between the sampled values. Finally, we screen out all data with ice crystal concentrations greater than $1/liter$ but we keep the aircraft data from the full cloud layer despite the limited lidar penetration depth. One of our objectives is to determine how representative of the whole cloud are the lidar solutions that are limited to the first 150-300 m.

Figures 2a-c compare the lidar-retrieved LWC histogram to the histograms derived from the various aircraft sensors for the same event as in Fig. 1. There is good agreement in the width of the distributions in all cases. The King and Nevzorov histograms tend to show a bimodal distribution with peaks at 0.05-0.08 and 0.26-0.29 g/m^3, respectively; the peaks differ slightly but that could be due to insufficient statistics. The lidar results show the same tendency but not quite as manifest. In addition, the lidar peaks occur at lower LWC values and the righthand side peak is broader and smoother. The principal differences occur at the middle-range and high values of 0.17-0.23 g/m^3 and 0.31-0.36 g/m^3, respectively. Nevertheless, the general qualitative agreement between the lidar and the two hotwire probe histograms is rather good. In the case of the size spectrometers data, Fig. 2c, the agreement is almost exact. However, the corresponding histograms for the effective droplet diameter plotted in Fig. 3 have more important differences. Both the lidar and the spectrometers histograms experience a maximum at ~ 16 μm but there is a sudden cutoff in the spectrometers values at 20 μm whereas the lidar histogram exhibits a longer tail extending to 40 μm.

We have performed similar histogram comparisons for all valid liquid-phase cloud events encountered in the AIRS experiment. The results are similar to those illustrated in Figs. 2 and 3. We summarize in Fig. 4 all comparisons in terms of scatter plots of the lidar solutions versus the *in situ* measurements for the LWC and the effective droplet diameter averaged over the duration of each event. These plots show a good correlation as well as a bias between the aircraft data and the lidar retrievals. The average slope of the lidar versus the *in situ* sensors is less than unity for the LWC and greater than unity for the effective diameter by an amount of 27% and 22%, respectively. In the case of the LWC, the slope is 0.90 ± 0.07 if we consider only the size spectrometers data, i.e. significantly closer to unity.

The non-unity slopes of Figs. 4a and b could be the result of the difference in the vertical extent of the cloud regions covered by the lidar and the aircraft probings; the lidar being limited to the first 150-300 m compared with the full layer for the aircraft. Indeed, it is not unreasonable to expect less LWC at the base of the clouds and a sedimentation of the larger droplets. We have therefore rerun the comparisons of Fig. 4 with a subset of aircraft data restricted to the first 300 m from cloud base. The resulting slope for the LWC is about the same as for the complete set, but it is reduced to 1.10 ± 0.08 for the effective droplet diameter. In the case of the LWC, there is one event with a large lidar-hotwire discrepancy that significantly lowers the average slope. If we remove the hotwire LWC data for that event, we find a slope of 0.92 ± 0.05, i.e. much closer to the ideal value of unity. Hence, it would seem that the agreement is indeed closer if we compare only data from the common cloud base layer. The improvement is in the right direction and confirms the consistency of the lidar solutions. There is justification for removing the hotwire data of that particular event because, if we were to assume that the hotwire measurements were correct, the lidar pulse would have penetrated to an optical depth of 9.6, which is incompatible with the dynamic range of our instrument.

The closer agreement obtained by restricting comparisons to the common cloud base layer is evidence for the validity of the lidar solutions. However, beyond that observation, the results of Figs. 1-4 suggest that the retrieved lidar solutions remain, with a precision of 20-30%, statistically representative of the whole cloud layer extending well above the pulse penetration depth, at least for the type of liquid-phase stratus clouds encountered in the AIRS program.

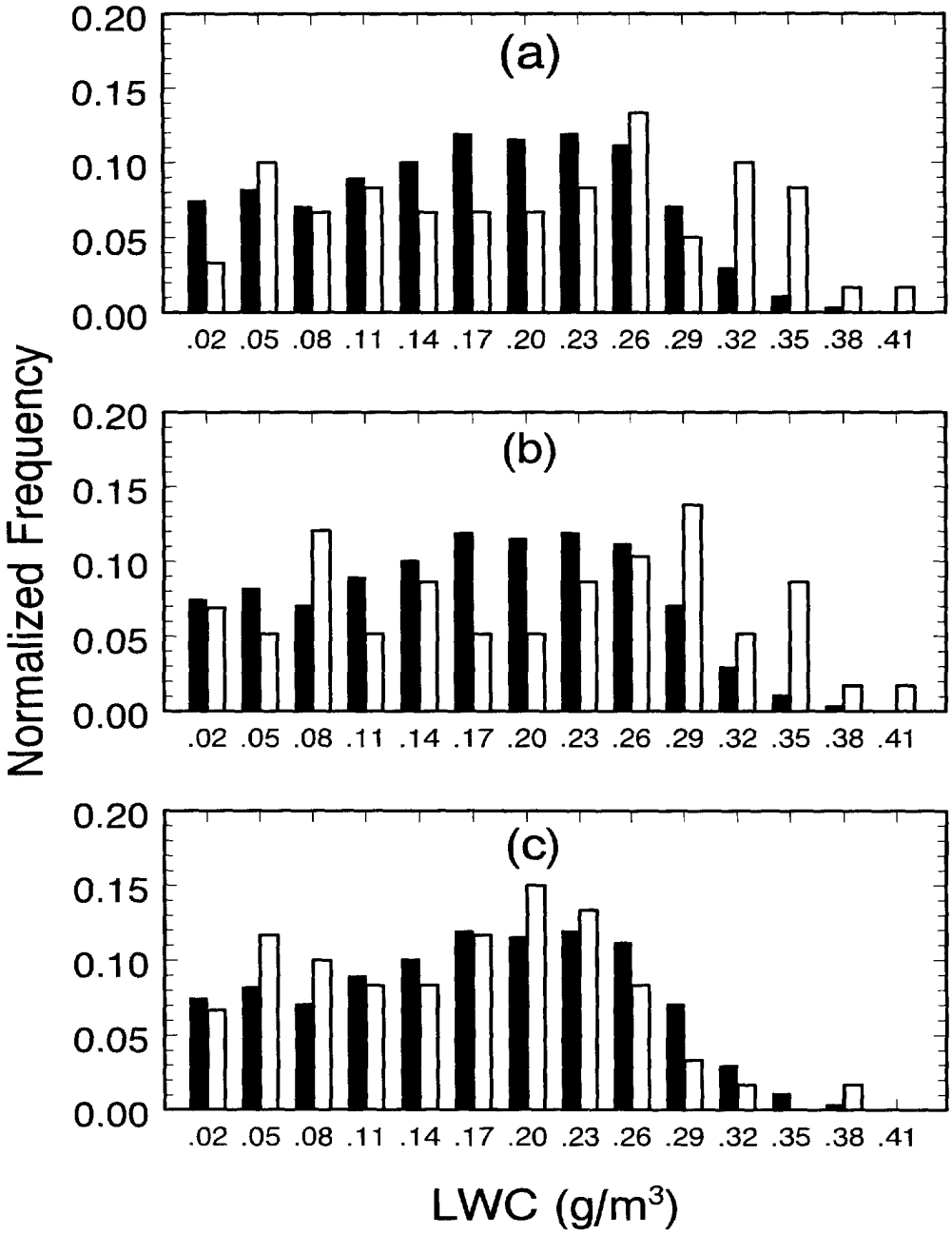

Figure 2. Comparison between LWC histogram constructed from lidar solutions (solid) and those obtained from *in situ* measurements (open) for the period 20h50-21h50 UTC on 3 December 1999. (a) King hotwire probe, (b) Nevzorov hotwire probe; and (c) size spectrometers

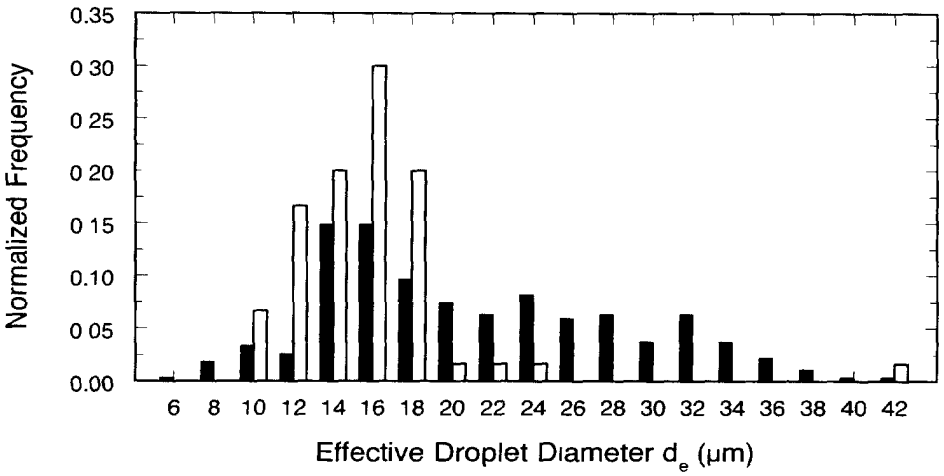

Figure 3. Comparison between effective droplet diameter histogram constructed from lidar solutions (solid) and that obtained from size spectrometers measurements (open) for the period 20h50-21h50 UTC on 3 December 1999

5. CONCLUSION

The comparison results of this report show that the MFOV lidar retrieval of microphysical parameters of liquid-phase clouds correlate well with *in situ* measurements. Good similarity is observed in the profiles and the histograms of the liquid water content and effective droplet diameter for the various events recorded in the AIRS program. There is, however, a bias between the lidar solutions and the *in situ* measurements. On average, the lidar-derived liquid water content is 25-30% less than the *in situ* data and the effective diameter, 20-25% greater. In the worst case, the bias is not significantly greater than between the hotwire probes and size spectrometers that were flown side by side. These differences are reduced to about 10% if we confine the aircraft data to the cloud base region, and screen out one event on account of incompatibility between the hotwire measurements of liquid water content and the recorded lidar penetration depth. Considering the many approximations made in constructing the lidar retrieval method and the independent error sources affecting the lidar and aircraft measurements, a 10% margin is very much acceptable.

One significant conclusion is that the lidar solutions are, within 20-30%, statistically representative of the complete layer in spite of the limited penetration range. If this observation is confirmed in other situations and cloud types, it certainly lessens the often raised objection of limited lidar sounding depth. Long-term MFOV lidar monitoring could thus become a viable, economical option for monitoring cloud microphysical and optical parameters. The addition of a microwave radiometer could provide the needed estimate of the full layer thickness by combining average liquid water content and integrated water column.

ACKNOWLEDGMENTS

We are grateful for the able technical assistance of Gilles Vallée and Sylvain Cantin. We also thank the authorities and personnel of Air Traffic Control at Montreal Mirabel Airport for their constant cooperation in the safe operation of the lidar.

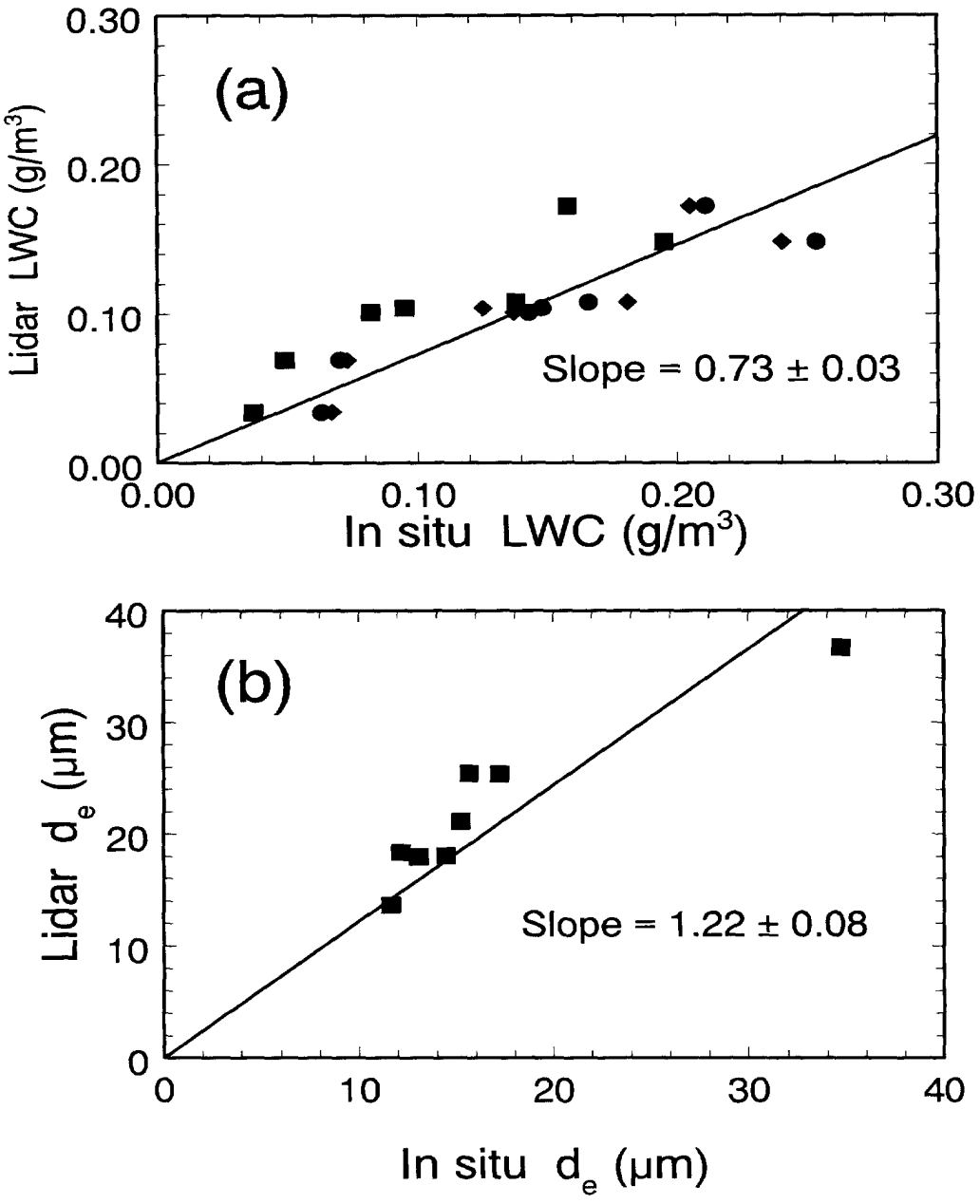

Figure 4. Scatter plot of lidar-derived versus full-layer *in situ* measurements of LWC (a) and effective droplet diameter (b). The plotted values are event averages. Solid disks for King probe; solid diamonds for Nevzorov probe; and solid squares for size spectrometers.

REFERENCES

1. K. Sassen. G.G. Mace, Z. Wang, M.R. Poellet, S.M. Sekelsky, and R.E. McIntosh, "Continental stratus clouds: a case study of coordinated remote sensing and aircraft measurements," J. Atmos. Sci., Vol. 56, pp. 2345-2358 (1999)
2. L.R. Bissonnette and D.L. Hutt, "Multiple scattering lidar", Appl. Opt., Vol. 29, pp. 5045-5046 (1990)
3. D.L. Hutt, L.R. Bissonnette, and L. Durand, "Multiple field of view lidar returns from atmospheric aerosols", Appl. Opt., Vol. 33, pp. 2338-2348 (1994)
4. L.R Bissonnette and D.L. Hutt, "Multiply scattered aerosol lidar returns: inversion method and comparison with *in situ* measurements", Appl. Opt., Vol. 34, pp. 6959-6975 (1995)
5. L.R. Bissonnette, G Roy, C. Bastille, and G. Vallée, "Lidar remote sensing of meteorological parameters in adverse weather: performance of electro-optic systems and aircraft in-flight icing," DREV Report-9707, October 1997
6. L.R. Bissonnette and G. Roy, "Lidar charactrization of cloud liquid water content and effective droplet diameter," SPIE Proceedings, Vol. 3865, pp. 160-171 (1999)
7. L.R. Bissonnette, G. Roy, G. Vallée, and S. Cantin, "Retrieval of cloud liquid water content and effective droplet diameter from multiply scattered lidar returns," SPIE Proceedings, Vol. 4087, pp. 939-946 (2000)
8. G. Roy, L.R. Bissonnette, C. Bastille, and G. Vallée, "Retrieval of droplet-size density distribution from multiple-field-of-view cross-polarized lidar signals," Appl. Opt., Vol. 38, pp. 5202-5211 (1999)
9. L.R. Bissonnette, P. Bruscaglioni, A. Ismaelli, G. Zaccanti, A. Cohen, Y. Benayahu, M. Kleiman, S. Egert, C. Flesia, P. Schwendimann, A.V. Starkov, M. Noormohammadian, U.G. Oppel, D.M. Winker, E.P. Zege, I.L. Katsev, and I.N. Polonski, "Lidar multiple scattering from clouds", Appl. Phys. B, Vol. 60, pp. 355-362 (1995)
10. E.W. Eloranta, "Practical model for the calculation of multiply scattered lidar returns," Appl. Opt., Vol. 37, pp. 2464-2472 (1998)
11. L.R. Bissonnette, G. Roy, S.G. Cober, and G.A. Isaac, "Lidar remote sensing of cloud liquid water content and effective droplet diameter: retrieval method and comparison wiyh *in situ* measurements," Defence Research Establishment Valcartier, Technical report under preparation (2001)
12. J.D. Klett, "Stable analytical inversion solutions for processing lidar returns," Appl. Opt., Vol. 20, pp 211-220 (1981)
13. G.A. Isaac, S.G. Cober, J.W. Strapp, D. Hudak, T.P. Ratvasky, D.L. Marcotte, and F Fabry, "Preliminary results from the Alliance Icing Research Study (AIRS)," AIAA 39th Aerospace Meeting and Exhibit, 8-12 January 2001, Reno, Nevada.

#517054

CA020298